Clay-coated sand grains in petroleum reservoirs: understanding their

distribution via a modern analogue

L. J. Wooldridge<sup>\*1</sup>, R. H. Worden<sup>\*2</sup>, J. Griffiths, J. E. P. Utley

<sup>1</sup>School of Environmental Sciences, University of Liverpool, Liverpool L69

3GP, UK

\*<sup>1</sup>Corresponding authors (e-mail: <u>luke.wooldridge@liv.ac.uk</u>)

\*<sup>2</sup>Corresponding authors (e-mail: <u>r.worden@liv.ac.uk</u>)

### ABSTRACT

2 Clay coated grains can inhibit ubiquitous, porosity-occluding quartz cement in deeply buried 3 sandstones and thus lead to anomalously high porosity. A moderate amount of clay that is distributed in sandstones as grain coats is good for reservoir quality in deeply buried 4 5 sandstones. Being able to predict the distribution of clay coated sand grains within petroleum 6 reservoirs is thus important to help find and exploit such anomalously good reservoir quality. 7 Here we have adopted a high resolution, analogue approach, using the Ravenglass Estuary 8 marginal-shallow marine system, in NW England, UK. Extensive geomorphic mapping, 9 grain size analysis and bioturbation intensity counts were linked to a range of scanning 10 electron microscopy techniques to characterise the distribution and origin of clay-coated sand 11 grains within surface sediment. Our work shows that grain coats are common within this 12 marginal-shallow marine system but they are heterogeneously distributed as a function of 13 grain size, clay fraction and depositional facies. The distribution and characteristics of 14 detrital-clay coated grains can be predicted with knowledge of specific depositional 15 environment, clay fraction percentage and grain size. The most extensive detrital-clay coated 16 grains are found within sediment composed of fine-grained sand containing 3.5 to 13.0 % 17 clay fraction, associated with inner estuary tidal flat facies. Thus, against common 18 convention, the work presented here suggests that, in deeply buried prospects, the best 19 porosity may be found in fine-grained, clay-bearing inner tidal flat facies sands and not in coarse, clean channel fill and bar facies. 20

# **INTRODUCTION**

22	Porosity and permeability generally decrease with increasing depth of burial in sandstones,
23	although a significant number of deeply buried sandstone reservoirs have unusually high
24	porosity and permeability (Bloch et al. 2002). Such anomalously high porosity and
25	permeability have most commonly been linked to the presence of chlorite clay coated grains
26	that inhibit the growth of porosity-occluding quartz cement (Ajdukiewicz and Larese 2012;
27	Ehrenberg 1993; Worden and Morad 2000).
28	The term clay coat encompasses both detrital and diagenetic origins (Ajdukiewicz and Larese
29	2012). Detrital-clay coated grains occur at or near the surface of the sediment, and are the
30	primary focus of this study.
31	Diagenetic clay coats either develop from the thermally-driven recrystallization of low-
32	temperature, detrital precursor clay coats or they grow in situ due to the authigenic alteration
33	of detrital or early diagenetic minerals interacting with the pore fluids during burial
34	(Ajdukiewicz and Larese, 2012; Wise et al., 2001; Worden and Morad, 2003).
35	Chlorite and illite clay coatings are considered to preserve reservoir quality by reducing the
36	nucleation area on detrital quartz grains that is available for authigenic quartz cementation
37	(Ehrenberg 1993; Pittman et al. 1992). Porosity can be at least 10 % higher than expected
38	where grain-coating clays are abundant (Ehrenberg 1993). Experiments undertaken by
39	Ajdukiewicz and Larese (2012); Billault et al. (2003) and Lander et al. (2008) led to the

40 conclusion that clay crystals within the clay coat act as barriers, inhibiting epitaxial quartz

41 cement growth and subsequent coalescence to form thick quartz overgrowths. The primary

42 factors controlling the effectiveness of clay coated grains for the inhibition of authigenic,

43 porosity-occluding quartz cement are the extent, completeness and distribution of the detrital

44 precursor clay coated grains (Billault et al. 2003).

45 Oil field-based studies which collectively show that clay coats are most common in fluvial to 46 marginal marine sediments including: Jurassic sandstones on the Norwegian continental shelf (Bloch et al. 2002), Jurassic-Triassic fluvial, lacustrine-deltaic sandstones of the Ordos basin, 47 48 China (Luo et al. 2009), marginal marine Jauf Formation, eastern Saudi Arabia (Al-Ramadan 49 et al. 2004), the Upper Cretaceous Tuscaloosa Formation, USA (Pittman et al. 1992), and see 50 review by Dowey et al. (2012). However there is no model capable of predicting the 51 occurrence of clay coated grains or the degree of completeness of grain coats within fluvial to marginal marine sediments. 52

53 The positive influence of chlorite and illite clay-coated grains on reservoir quality in deeply 54 buried sandstone has resulted in extensive reservoir core-based research (Ajdukiewicz et al. 55 2010; Gould et al. 2010; Pittman et al. 1992) and laboratory experiments (Ajdukiewicz and Larese 2012; Billault et al. 2003; Pittman et al. 1992). Chlorite coated grains have been 56 57 observed to inhibit quartz cement and the need to understand the origin of chlorite coated 58 grains was the driving force that led to the current study. Notable chlorite clay coated 59 reservoir units include the Tilje Formation, Norwegian continental shelf (Ehrenberg 1993), 60 Tuscaloosa Formation, U.S. Gulf Coast (Ajdukiewicz and Larese 2012) and the Rotliegend 61 Sandstone, northern Netherland (Gaupp and Okkerman 2011). Sandstones which contain 62 illite and mixed layer illite-smectite clay coated grains have been less commonly advocated 63 but include the Garn Formation, Mid-Norway (Storvoll et al. 2002), Williams Fork 64 Formation, Colorado (Ozkan et al. 2011) and Jauf Formation, Eastern Saudi Arabia (Al-65 Ramadan et al. 2004; Cocker et al. 2003). 66 Aagaard et al. (2000) showed that low temperature, discontinuous, detrital-clay coated grains 67 recrystallized during experiments at 90 °C to form thick, continuous, diagenetic clay coats that are morphologically consistent with naturally occurring reservoir examples. In some 68

69 examples, euhedral clay minerals grow out into the pore from an underlying, unstructured

70	clay coat (Gould et al. 2010). Such clay coat stratigraphy could be the result of a detrital, or
71	very early diagenetic, clay coat acting as a seed for deep burial diagenetic clay coat
72	neoformation.

73	Despite the importance of being able to predict the occurrence and distribution of detrital-
74	clay coated grains, there is no all-encompassing model that is useful for ranking prospects or
75	populating reservoir models with the completeness of clay coats in marginal marine
76	sandstones. Relatively little fundamental work has been undertaken on the controls on clay
77	coat growth in sediments although Wilson (1992) and Matlack et al. (1989) undertook early
78	studies focused upon environments (aeolian, marine-shelf, marginal marine, fluvial) in which
79	clay-coated sand grains occur and potential mechanisms of formation (bioturbation,
80	infiltration, inheritance). In order to predict anomalously high porosity in the subsurface,
81	there is a need to focus on the origin and spatial distribution of detrital-clay coated grains
82	since clay coats inhibit quartz cement in deeply buried sandstones (Bloch et al. 2002)
83	Anomalously high porosity has also been shown to derive from other possesses such as early
84	oil charge, over pressure and microquartz coatings (Bloch et al. 2002).
85	The four main ways to develop a fundamental understanding of primary sedimentary
86	environment and mineral distribution, and thus the processes that lead to clay coats, are: core-
87	based studies, outcrop based studies, experimental studies and modern analogue studies.
88	Core based studies have problems of limited spatial resolution of samples (wide spacing
89	between wells and the lack of abundant cores in most fields) and the abiding uncertainty
90	about both the primary mineralogy and exact environment of deposition due to subsequent
91	diagenetic modifications. Outcrop based studies overcome the spatial resolution problem but
92	typically suffer from weathering-related recent changes to mineralogy, plus outcrop-
93	diagenesis studies routinely have problems in seeing through the long history of burial,
94	heating and then uplift. We have here adopted a modern analogue approach, linking the

95	distribution of detrital-clay coated grains to sedimentary processes and characteristics (grain
96	size, percentage clay fraction) and biological processes (bioturbation). The detailed study of
97	sediment from modern environments permits a high resolution investigation into the
98	distribution of detrital-clay coated grains, removing the limited spatial distribution,
99	stratigraphic coverage and ambiguous depositional environment interpretations of subsurface
100	core-based studies. This study addresses the following questions, focussed on the marginal-
101	shallow marine Ravenglass Estuary system (Fig. 1).
102	1. What are the textural characteristics of detrital-clay coated grains within a
103	modern marginal-shallow marine setting?
104	2. What are the mineralogical characteristics of clay-coated sand grains within a
105	modern marginal-shallow marine setting?
106	3. How variable is the coverage of detrital-clay coated grains within a modern
107	marginal marine system?
108	4. What controls the formation and distribution of detrital-clay coated grains?
109	5. Are the clay coats in this modern, marginal-shallow marine system, texturally
110	comparable to other modern or subsurface examples?
111	6. What is the potential impact of using modern analogues for the prediction of
112	reservoir quality in ancient and deeply buried sandstones from the same
113	primary environment?
114	STUDY SITE GEOMORPHOLOGY
115	The Ravenglass Estuary is located in Cumbria, NW England. The mid to upper portions of
116	the Ravenglass Estuary are fed by three rivers the Esk, Mite and Irt, with the lower, western
117	part of the estuary connected by a single channel to the Irish Sea (Bousher 1999) (Fig. 1).
118	Ravenglass sediment is quartz-dominated (Daneshvar 2011; Daneshvar and Worden 2016)

119 with depositional environments translatable to marginal-shallow marine petroleum reservoirs.

120 Ravenglass is a modern analogue equivalent to the environment of deposition for many

ancient and deeply buried, chlorite-coated sandstone reservoirs such as the tidally-influenced,

shallow marine-deltaic Tilje Formation, Norway (Ehrenberg 1993), braid delta margin with

123 foreshore and shoreface deposits Garn Formation, Norway (Storvoll et al. 2002), and

shallow-marine to deltaic Lower Vicksburg Formation, USA (Grigsby 2001).

125 The 5.6 km<sup>2</sup> estuary has a maximum tidal range of 7.55 m and is 86% intertidal (Bousher

126 1999; Lloyd et al. 2013). The estuary has extensive back barrier tidal flats and tidal bars,

127 fringed by well-established saltmarsh vegetation (Bousher 1999). The estuary is connected to

the Irish Sea through a single, 500m wide, tidal inlet that dissects a fringing coastal barrier

129 which is topped with eolian dunes. The three fluvial channels, fluvial overbank, foreshore

and ebb delta complex provide a complete fluvial to marine transect that we have investigated

in terms of depositional environments, and detrital-clay coat abundance, with analysis of

detrital-clay coat mineralogy (Fig. 1). Despite the high spring tidal range, the estuary

133 contains geomorphological elements consistent with a mixed energy (wave-tide) regime,

following the estuary classification scheme proposed by Ainsworth et al. (2011). This

135 indicates a tidal hydrodynamic dominance within the inner estuary and wave-dominated

136 processes occurring along the foreshore coastal side of the barrier spits.

137 The marginal- shallow marine Ravenglass system can be divided into fluvial-, estuary-,

shallow marine- and eolian dune-dominated regimes, with the results of this study subdivided

139 by sub-environment. The estuary has a clay mineral sediment assemblage consisting of

140 chlorite, illite and kaolinite, largely derived from suspended fluvial sediment, originating

141 from incision and weathering of the hinterland geology (Daneshvar 2011; Daneshvar and

- 142 Worden 2016). The southern River Esk drains the Palaeozoic Eskdale Granite; the northern
- 143 River Irt drains the Triassic Sherwood Sandstone Group and the Borrowdale Volcanic Group;

144	the central, but minor, River Mite drains a combination of Eskdale Granite, Triassic
145	Sherwood Sandstone Group and the Borrowdale Volcanic Group (Moseley 1978).
146	MATERIALS AND METHODS
147	Field-Based Mapping of the Estuary
148	The estuary was initially mapped by identifying each depositional environment via world
149	imagery and Google Earth. Extensive field mapping and sampling of all geomorphological
150	elements enabled ground-truthing of mapped depositional elements and interpolation using
151	ArcGIS. Tidal flats were further subdivided using the scheme proposed by Dyer (1979),
152	based upon component volume clay fraction (< 2 $\mu$ m fraction):
153	0-10 % clay fraction is classed as sand flat,
154	10-30 % is muddy sand flat,
155	30-80 % is sandy mud flat.
156	Surface sediment grain size (approximately 2 cm depth) was determined at 3151 sites in the
157	field using grain size cards and mapped using interpolated in ArcGIS. Lugworm faecal cast
158	density (number per square metre) was recorded in the field using a 1m <sup>2</sup> quadrat, randomly
159	thrown at 3182 sites within the estuary. Lugworm density was mapped across the entire
160	intertidal exposed area, and also mapped using interpolated in ArcGIS. Polished thin sections
161	were constructed from samples across a tidal flat succession to allow mineralogical
162	quantification via automated scanning electron microscope-energy dispersive spectrometry
163	(SEM-EDS). Sediment clay fraction mineralogy was established through X-ray diffraction
164	analysis (XRD).

# Determination of Clay Coat Coverage

This study is primarily focused on a suite of 181 surface sediment samples which were
subject to grain coat petrography. The sample sites were chosen to provide sufficient spatial
coverage and to encompass a fluvial- shallow marine transect incorporating all depositional
environments. The clay size fraction volume (weight percentage) was established for 95 of
the 181 sites.

Approximately 50 cm<sup>3</sup> of surface sediment was collected at each of the 181 sites. The sediment was then sub-sampled and dried at room temperature. Quantification of detrital clay coverage was achieved using scanning electron microscope (SEM) analysis of grain mounts on a 1 cm diameter stub. The grain mount stubs were examined by SEM petrography in backscattered electron (BSE) imaging.

176 A complete traverse across each SEM stub was collected by stitching together nine or more 177 BSE images taken for each sample to produce a representative image of approximately 200 178 grains. In comparison to thin-section based approaches for the study of grain coats, this 179 approach permitted the investigation of detrital-clay coated grains in three dimensions. It 180 also allowed for detailed classification of each sample (Fig. 2). Here we have adopted a 181 novel approach that initially categorises the samples in terms of absence (group 1) or 182 presence (groups 2-5) of clay coat and then subdivides those with coats into the degree of 183 coat coverage (by surface area). Detrital-clay coats within this study were thus categorised 184 into five principle classes:

185 1) Complete absence of attached clay coats.

186 2) Less than half of the grains have a small (~ 1-5 %) surface area of attached clay coats.

187 3) Every grain exhibits at least ~ 5-15 % surface area of attached clay coats.

4) Clay coats observed on every grain with the majority exhibiting extensive (~ 15-30 %)

surface area grain coverage.

190 5) Extensive > 30 % surface area covered by clay coats observed on every grain.

191	To ensure reliability of the method and interpretation, duplicate SEM stub preparation and
192	analysis was undertaken for 38 of the 181 samples to check the consistency of the
193	classification method. We here note that all replicates faithfully reproduced the initial
194	classification. Critical point drying (Jernigan and McAtee 1975) was not applied to the
195	samples, owing to the absence of delicate fibrous clays associated with authigenic growth.
196	Clay coat mineralogy
197	Mineralogical quantification of clay coated sand grains from a mixed sand-mud tidal flat was
198	undertaken via SEM-EDS using an FEI-QEMSCAN® (Armitage et al. 2016). This approach
199	was selected to enable in-situ imaging of clay mineralogy, distribution characteristics and
200	define the link between sediment clay mineralogy and that of clay coats. Three polished thin
201	sections were constructed from surface sediment. The QEMSCAN® system comprises a
202	scanning electron microscope coupled with fast energy dispersive spectrometers (EDS), a
203	microanalyzer and an electronic processing unit, which integrates the data to provide
204	information about the micron scale texture, chemical and mineral composition. The step size
205	for the analysis was 1 $\mu$ m to ensure that the fine fraction in the sediment was analyzed as well
206	as framework grains.
207	The data are presented as a combination of a backscatter secondary electron image, and fully
208	quantitative mineralogical content image (framework grains) and quantitative clay
209	mineralogy (total clay, illite, chlorite, kaolinite) to represent the sediment assemblage and
210	component clay-coated sand grains.
211	Determination of clay fraction
212	The percentage of the clay fraction ( $< 2 \mu m$ ) was established via homogenised sediment sub-
213	samples, dried at 60°C. A few grams of sample were added to 200ml of water and then

215	removed sand and silt sized particles, with the supernatant water (containing the clay grain
216	sized particles) decanted and settled by centrifugation to obtain the clay fraction. The
217	separated clay fraction was dried at 60°C, crushed in an agate pestle and mortar and then
218	weighed, revealing the percentage clay fraction within the sediment sample.
219	Determination of bulk sediment clay fraction mineralogy
220	Classification of the clay fraction (<2 $\mu$ m) mineralogy was undertaken by X-ray diffraction
221	analysis (XRD). The clay sized fraction was detached from framework grains using an
222	ultrasonic bath and isolated using centrifuge settling, at 5000 rpm for 10 minutes. The
223	separated clay fraction was dried at 60 degrees and scanned as a randomly orientated powder,
224	using a PANalytical X'Pert Pro MPD X-ray diffractometer. XRD analysis was carried out
225	for the same samples that were mineralogy mapped through (SEM-EDS) analysis.
226	RESULTS
226	RESULTS
226	<b>KESULIS</b> Surface Sedimentary Characteristics and Distribution of Biological Activity
227	Surface Sedimentary Characteristics and Distribution of Biological Activity
227 228	Surface Sedimentary Characteristics and Distribution of Biological Activity Sedimentary environments were identified in the field, with further subdivision of the tidal
227 228 229	Surface Sedimentary Characteristics and Distribution of Biological Activity Sedimentary environments were identified in the field, with further subdivision of the tidal flats based upon the lab-derived clay fraction data sets into sand-flat, muddy sand-flat and
227 228 229 230	<i>Surface Sedimentary Characteristics and Distribution of Biological Activity</i> Sedimentary environments were identified in the field, with further subdivision of the tidal flats based upon the lab-derived clay fraction data sets into sand-flat, muddy sand-flat and sandy mud-flat (Fig. 1).
227 228 229 230 231	Surface Sedimentary Characteristics and Distribution of Biological Activity Sedimentary environments were identified in the field, with further subdivision of the tidal flats based upon the lab-derived clay fraction data sets into sand-flat, muddy sand-flat and sandy mud-flat (Fig. 1). High resolution, spatial distribution maps of sediment grain size reveal a wide range of mean
227 228 229 230 231 232	Surface Sedimentary Characteristics and Distribution of Biological Activity Sedimentary environments were identified in the field, with further subdivision of the tidal flats based upon the lab-derived clay fraction data sets into sand-flat, muddy sand-flat and sandy mud-flat (Fig. 1). High resolution, spatial distribution maps of sediment grain size reveal a wide range of mean grain sizes, from very fine to coarse sand sized sediment (Fig. 3A). There is a large scale
227 228 229 230 231 232 233	Surface Sedimentary Characteristics and Distribution of Biological Activity Sedimentary environments were identified in the field, with further subdivision of the tidal flats based upon the lab-derived clay fraction data sets into sand-flat, muddy sand-flat and sandy mud-flat (Fig. 1). High resolution, spatial distribution maps of sediment grain size reveal a wide range of mean grain sizes, from very fine to coarse sand sized sediment (Fig. 3A). There is a large scale trend of decreasing grain size away from the ocean, and smaller scale patterns of decreasing
227 228 229 230 231 232 233 233	Surface Sedimentary Characteristics and Distribution of Biological Activity Sedimentary environments were identified in the field, with further subdivision of the tidal flats based upon the lab-derived clay fraction data sets into sand-flat, muddy sand-flat and sandy mud-flat (Fig. 1). High resolution, spatial distribution maps of sediment grain size reveal a wide range of mean grain sizes, from very fine to coarse sand sized sediment (Fig. 3A). There is a large scale trend of decreasing grain size away from the ocean, and smaller scale patterns of decreasing grain size with increasing distance from the main ebb channel, towards the tidal limit (Fig.

238	taken to indicate the intensity of bioturbation in the biotic zone of the sediment (McIlroy et
239	al. 2003; Needham et al. 2005). The highest density of lugworms (31 to $> 50$ per m <sup>2</sup> ) was
240	observed within the outer sand tidal flats and non-vegetated tidal bar depositional
241	environments (Figs. 1 and 3C). Comparing the sediment grain size map (Fig. 3A) to the
242	lugworm population map (Fig. 3B) suggests that well-developed lugworm populations tend to
243	be confined predominantly to the inner estuary where the sediment grain size tends to be
244	between 88 and 177 μm.
245	The percentage sediment clay fraction data have been split into eight classes (Fig. 3B).
246	Samples that contain $> 1.5$ % clay fraction are confined to the inner estuary. Samples that
247	contain $< 1.5$ % clay fraction sit within the seaward portion of the estuary and outer tidal-flats
248	(Fig. 3B). This pattern suggests that there is an inverse relationship between overall grain
249	size and the amount of co-deposited clay fraction, i.e. there is an increased percentage of the
250	clay fraction with decreasing grain size.
251	Clay fraction mineralogy
251 252	Clay fraction mineralogy The sediment samples have a clay fraction composed of illite, chlorite and kaolinite, with an
252	The sediment samples have a clay fraction composed of illite, chlorite and kaolinite, with an
252 253	The sediment samples have a clay fraction composed of illite, chlorite and kaolinite, with an average 7.6 % clay fraction in the sediment . X-ray diffraction shows that the clay fraction is
252 253 254	The sediment samples have a clay fraction composed of illite, chlorite and kaolinite, with an average 7.6 % clay fraction in the sediment . X-ray diffraction shows that the clay fraction is dominated by illite (62 % of the clay fraction) clay with chlorite (17 % of the clay fraction)
252 253 254 255	The sediment samples have a clay fraction composed of illite, chlorite and kaolinite, with an average 7.6 % clay fraction in the sediment . X-ray diffraction shows that the clay fraction is dominated by illite (62 % of the clay fraction) clay with chlorite (17 % of the clay fraction) and kaolinite (21 % of the clay fraction) expressing similar values. (Fig.4).
252 253 254 255 256	The sediment samples have a clay fraction composed of illite, chlorite and kaolinite, with an average 7.6 % clay fraction in the sediment . X-ray diffraction shows that the clay fraction is dominated by illite (62 % of the clay fraction) clay with chlorite (17 % of the clay fraction) and kaolinite (21 % of the clay fraction) expressing similar values. (Fig.4). <i>Characteristics of Detrital-clay coats</i>
252 253 254 255 256 257	The sediment samples have a clay fraction composed of illite, chlorite and kaolinite, with an average 7.6 % clay fraction in the sediment . X-ray diffraction shows that the clay fraction is dominated by illite (62 % of the clay fraction) clay with chlorite (17 % of the clay fraction) and kaolinite (21 % of the clay fraction) expressing similar values. (Fig.4). <i>Characteristics of Detrital-clay coats</i> The observed detrital-clay coated grains are generally characterised by thin and discontinuous
252 253 254 255 256 257 258	The sediment samples have a clay fraction composed of illite, chlorite and kaolinite, with an average 7.6 % clay fraction in the sediment . X-ray diffraction shows that the clay fraction is dominated by illite (62 % of the clay fraction) clay with chlorite (17 % of the clay fraction) and kaolinite (21 % of the clay fraction) expressing similar values. (Fig.4). <i>Characteristics of Detrital-clay coats</i> The observed detrital-clay coated grains are generally characterised by thin and discontinuous accumulations of individual but interlocking (overlapping and aligned clay platelets) clay
252 253 254 255 256 257 258 259	The sediment samples have a clay fraction composed of illite, chlorite and kaolinite, with an average 7.6 % clay fraction in the sediment . X-ray diffraction shows that the clay fraction is dominated by illite (62 % of the clay fraction) clay with chlorite (17 % of the clay fraction) and kaolinite (21 % of the clay fraction) expressing similar values. (Fig.4). <i>Characteristics of Detrital-clay coats</i> The observed detrital-clay coated grains are generally characterised by thin and discontinuous accumulations of individual but interlocking (overlapping and aligned clay platelets) clay minerals (Fig. 5). This study has focussed on the morphology of the coat and here we do not

262	grains that contain coats) (Figs. 2). The clay coats occur on both convex and concave grain
263	faces but the coats with the greatest thickness (maximum of about 5 $\mu$ m) occur in grain
264	indentations (Fig. 5G, 6E, 7). Clay coats occupy up to about 60 % surface area of individual
265	grains in a given sample.
266	Detrital-clay coats are composed of individual interlocking clay minerals with a mixed
267	mineralogy even along a singular ridge structure and a range of accessory impurities
268	consisting of silt-sized quartz and bioclastic debri. Clay coats have been observed on all
269	component framework grains within the sediment assemblage (quartz, feldspar, dolomite,
270	calcite). The sand grains within this study are coated with a mixture of clay minerals (Fig. 7),
271	dominated by illite (9.1 image area percentage), with minor chlorite (1.7 image area
272	percentage) and kaolinite (1.1 image area percentage). There was no identified variability
273	between clay mineralogy and component clay coat morphological classes (ridged, bridged,
274	and clumped).
275	Detrital-clay coats occur with a variety of morphologies (Fig. 5). Here, we have grouped the
276	samples into three principle morphological classes: ridged, bridged and clumped (Fig. 6).
277	Ridged clay coats consist of elongate intergrowths of plate-like clay minerals, orientated at
278	high angles to the grain surface (Fig. 6A). Ridged coats have variable lengths (< 200 $\mu$ m)
279	and are preferentially observed upon relatively flat grain surfaces with minimal (silt)
280	impurities. Ridged clay coated grains predominantly occur within the coarser, cleaner
281	sediment assemblages that are associated with outer tidal flat and non-vegetated tidal bar
282	environments.
283	Bridged clay coat textures occur between detrital grains. Bridged clay coats consist of
284	elongate clay mineral aggregates that connect two grains. Bridged clay coats are relatively

uncommon within surface sediment, possibly as result of the sampling procedure (Fig. 6B).

286 Clumped clay coats are highly variable both in extent and thickness (Fig. 5 and 6C).

287 Clumped coatings are commonly reach sizes of up to 200 µm, and contain silt-sized

288 fragments as well as clay grade material. Clumped clay coats are most abundant within the

289 upper estuary intertidal muddy sand flats, tidal bars and salt marsh depositional

environments.

291

290

## Spatial Distribution of Detrital-Clay Coated Grains

292 There is a high degree of variability in the distribution of detrital-clay coated grains, although 293 most outer estuary sediment exhibits no more than minor attached clay coats (Fig. 8). The 294 proportion of detrital-clay coated grains in the estuary tends to increase with distance from 295 the open ocean and with distance from the main ebb channel. Clay coats are most extensive 296 within the upper reaches of the three estuary channels. There is a strongly heterogeneous 297 distribution of clay coat classes within the southern Esk estuary arm, while the northern Irt 298 and central Mite estuary arms show more homogeneous distributions. In the central and sea-299 ward portions of the estuary, clay coats tend to be either absent or present in trace amounts 300 (classes 1 and 2).

301 The surface sediment samples have here been plotted against depositional environment, with 302 the aim of allowing the modern clay coat data to be compared to ancient, deeply buried 303 sediments (Fig. 9). Detrital-clay coated grains are present within the fluvial channel 304 sediments ranging from absent (class 1) to extensive (class 4) depending upon the position of 305 the sample relative to the channel axis. Grains from inner meander and point bars samples 306 typically have better developed clay coats representative of class 3-4. Grains from fluvial 307 overbank samples tend to have the best developed detrital-clay coats on grains (class 3-5). 308 Inner estuary tidal depositional environments have a heterogeneous pattern of detrital-clay 309 coated grain coverage. Clay coats are more extensively developed on detrital grains within

310 vegetated, as opposed to non-vegetated, tidal bars (Fig. 9). Tidal flats (sand flat, muddy sand 311 flat, sandy mud flat) represent the only inner estuary depositional environment in which the 312 full spectrum of clay coat grain coverage has been observed (classes 1 to 5). Samples that 313 contain >10% clay fraction correspond to muddy sand flats. All grains in all samples from 314 muddy sand flats contain some degree of clay coating. Samples from sandy mud flat (with 315 >30% clay fraction) contain extensive (class 4-5) detrital-clay coat grain coverage. Saltmarsh 316 sediment assemblages have uniformly well-developed detrital-clay coats (class 5). The 317 observed variability in detrital-clay coat characteristics within tidal environments correlates 318 to grain size; the more extensively developed detrital-clay coats (class 4-5) occur within very 319 fine sand grain size dominated sediment (e.g. compare Fig. 8 to Fig 3A). 320 The samples from foreshore, ebb delta, tidal inlet and eolian dune depositional environments 321 largely do not contain detrital-clay coated grains. Most samples from the vegetated, dune-322 topped spits and sheltered region within the tidal inlet contained no clay coat coverage (class 323 1) and the remainder had minor clay coat coverage (class 2) (Fig. 9). Detrital-Clay Coated Grains: Grain Size, Clay Fraction and Bioturbation 324 325 Bin class intervals have been plotted against average grain size, percentage clay fraction and 326 lugworm density (Fig. 10). This confirms that there is increasing percentage clay fraction 327 with decreasing grain size. This also shows that increasing the percentage of the clay fraction 328 correlates with increasing clay coat coverage (class number). Thus, clay coat class 3 (every 329 grain exhibiting at least ~5-15 % attached clay coats) corresponds to sediment with a 2.5% 330 clay fraction, while clay coat class 5 (extensive, >30 %, clay coats observed on every grain) 331 corresponds to sediment with 10% clay fraction (Fig. 10). The coverage of clay coats does 332 not seem to simply relate to lugworm density with the two highest clay coat classes found in 333 association with low lugworm densities (Fig. 10).

334	Detrital-clay coats vary systematically within a given depositional environment (Fig. 9).
335	Extensive detrital-clay coated grains are observed within the inner estuary tidal depositional
336	environments, and they increase in extent towards the upper tidal limit (Figs. 8 and 9).
337	Variations in grain size and clay fraction are secondary controls, with a lower fine sand grain
338	size and >5 % clay fraction required to form uniform-extensive detrital-clay coats upon
339	grains (class 3-5). There are negligible attached clay coats (class 1-2) observed within the
340	high energy (upper fine-lower medium grain size), clean (<2% clay fraction) sand
341	assemblages of the outer sand tidal flat, foreshore, ebb delta and eolian dune environments.

w sustamatically within a siver densitienal environment (Fig. 0)

342

224

Detritel

#### DISCUSSION

343 Origin of Detrital-clay coat Textures

344 The internal fabric and outer morphology of clay coats in deeply buried reservoir have been 345 described in a few studies. Clay coats tend to be composed of an inner, densely packed, 346 tangentially oriented, root layer that tends to be overlain by an outer coat composed of 347 perpendicular euhedral flakes that grow into open pore spaces (Ajdukiewicz and Larese 2012; 348 Wise et al. 2001). It has been proposed that the inner layers are the result of thermally-driven 349 recrystallization of precursor detrital-clay coats (Aagaard et al. 2000; Billault et al. 2003). 350 The clay coats from the Ravenglass Estuary, described here, are therefore analogues for the 351 inner layer of clay coats reported from deeply buried reservoirs. 352 The observed ridged and bridged textures within this study (Fig. 6A, B, 7) have been reported 353 previously in a range of case studies (Dowey 2013; Franks and Zwingmann 2010; 354 Houseknecht 1992; Matlack et al. 1989; Moraes and De Ros 1992; Wilson 1992) and in 355 synthesis experiments (Matlack et al. 1989). Ridged detrital-clay coat textures have been 356 interpreted to derive from infiltration processes (Wilson 1992); bridge structures have been 357 reported to form where ridges join two adjacent grains; initially bridged structures develop

distinct ridged texture when the sediment is disaggregated (Matlack et al. 1989). The

359 sediment from the Ravenglass Estuary exhibits many of the textural characteristics that have

been reported to result from clay infiltration into sand-dominated sediment (Wilson 1992).

361 Infiltrated ridged detrital-clay coat textures have been reported within the Brazos River and

362 Galveston marginal marine system, Texas (Matlack et al. 1989), as well as in the Anllons

363 Estuary, Spain and Leiravogur Estuary, Iceland (Dowey 2013).

364 Infiltration occurs when water that contains suspended clay and silt flows into partially water-

saturated sandy sediment. Within estuarine settings, infiltration is driven by a hydraulic

366 gradient produced by the effect of the tidal range. This gradient drives suspended clay

through the sediment at falling tide, towards the low tidal main ebb channel or during times

of flooding due to increased rainfall in the hinterland (Santos et al. 2012). Reduction of flow

velocity results in the deposition of the suspended clay and silt particles on to the sand grains

370 (Dowey 2013; Worden and Morad 2003).

371 Clumped clay coat textures, that are comparable to those illustrated in this study (Fig. 6C),

have been reported within the sediment of the Mandovi Estuary, India (Mohan Kessarkar et

al. 2010), with similar clump sizes and textures. The subtropical Mandovi Estuary clay coats

are composed of clay particles, bioclasts and organics that produce a heterogeneous

375 mineralogy that is reported to be fluvially-derived from weathering products in the hinterland

376 (Mohan Kessarkar et al. 2010). Clumped clay accumulations have also been reported within

the fluvial-estuarine Rappahannock River, Virginia (Pierce and Nichols 1986). In both the

378 Rappahannock and Mandovi examples, clumped textures were interpreted to originate from

the deposition of biogenic (faecal) pellets and flocculated estuarine aggregates (Crone 1975)

under stagnant pore water conditions in the estuary.

381 A comparison of clay coat textures found in the Ravenglass Estuary to other modern

analogues, as well as experimental-based results, suggests that clay coats derive from a

combination of infiltration, resulting in the ridged-bridge textures, and flocculation with the
deposition of biogenic faecal pellets resulting in clumped textures.

# 385 Origin of detrital-clay coat mineralogy: internal or external to the estuary?

386 The illite-dominated, mixed mineralogy of the clay-coated sand grains, determined by

spatially-resolved SEM-EDS (Fig. 7), is consistent with the clay fraction mineralogy

identified by XRD (Fig. 4). Had the clay coats formed in the hinterland, a much more varied

389 clay-coat mineralogy would be expected than revealed by micro-studies using SEM-EDS and

390 bulk-studies using XRD. Therefore, the observation that the clay coat mineralogy reflects the

bulk clay mineralogy of the estuary implies that the clay coats were formed in the estuary

- itself rather than in the hinterland.
- 393

## Detrital-Clay Coat Distribution and Origin

394 It has been reported that the primary depositional environment of a clastic sediment exerts a 395 strong control on subsequent diagenetic processes, via the sediment texture, primary 396 mineralogy, organic content and aqueous chemistry (Ehrenberg 1997; Morad et al. 2010; 397 Worden and Morad 2003). The concept of a depositional control on the occurrence, type and 398 subsequent diagenetic evolution of detrital-clay coats is reasonably well established (Bloch et 399 al. 2002; Dowey et al. 2012; Ehrenberg 1993; Luo et al. 2009; Matlack et al. 1989). The 400 results of this study confirm a depositional environment control but reveal, for the first time, 401 systematic variability of the extent and completeness of clay coat coverage on a marginal 402 marine depositional sub-environments scale.

403

### Comparison of Clay Coats in Ravenglass to Modern Estuary Studies

In the Ravenglass marginal-shallow marine system, the most extensive detrital-clay coated
grains are confined to the inner estuary tidal flat, tidal bar, saltmarsh and fluvial point bar

406 depositional environments. In contrast, detrital-clay coated grains are effectively absent 407 within the coarse, clean sand that is associated with outer tidal flats, foreshore, dune topped 408 spits, fluvial channel axis and main ebb channels. The distributions that are illustrated in 409 Figures 8 to 10 have similarities to that of detrital-clay coated grain distribution along the 410 Texas Gulf Coast, Galveston and within the Brazos River (Matlack et al. 1989). The Texas 411 study reported clay coated grains from fluvial point bars, but an absence of detrital-clay 412 coated grains within beach, delta beach, flood tidal delta, and delta plain surface sediments. 413 Studies of the Anllons Estuary, Spain and Leiravogur Estuary, Iceland undertaken by Dowey 414 (2013), support the observed distribution within this study, with detrital-clay coated grains 415 being best developed within the less marine-influenced, middle and upper estuary reaches 416 related to muddy tidal flats.

# 417 Comparison of Ravenglass Clay Coats to Ancient, Deeply Buried Clastic 418 Sediment

Reservoir studies, based on cored wells and interpretation of primary depositional
environments, tend to be hampered by a lack of high resolution facies interpretation and
relatively poor definition of the spatial and stratigraphic distribution of clay coated grains.
To date, there is no published subsurface reservoir dataset that compares to the high spatial
resolution and the complete certainty of the depositional environment used in this modern
analogue study.

Although morphologically dissimilar, occurring as discontinuous clumps and ridges, broad
textural and mineralogical similarities are identifiable between the precursor detrital-clay
coats of this study and clay coats in diagenetically-altered reservoirs. Mixed mineralogy has
been reported in several reservoirs, for example the Lower Cretaceous Mississauga
Formation (Gould et al. 2010) and the Jurassic Garn formation (Storvoll et al. 2002), in which

430 the inner (tangential) diagenetic clay coats consist of a mixed illite-chlorite- mineralogy that 431 is broadly similar to the mixed mineralogy of the detrital-clay coats in Ravenglass (Fig. 7). 432 In the Upper Carboniferous submarine-fan and marine slope facies of the Arkoma Formation, 433 USA it has been reported that muddy clay coated grain facies offer the best reservoir quality 434 prospects compared to the well-sorted, clean sandstones (with little or no dispersed clays). 435 (Houseknecht 1992). In the Arkoma Formation, amalgamated sandstone units contain beds 436 with clay coated grains and no quartz overgrowth and adjacent clean sandstone beds that are 437 devoid of clay coated grains but with pervasively quartz overgrowth, and therefore have 438 negligible remaining porosity (Houseknecht 1992). Although the environment of deposition 439 is different, the Arkoma example illustrates that a small quantity of clay that is co-deposited 440 with sand can lead to improved reservoir quality.

# 441 CONTROLS ON THE FORMATION AND DISTRIBUTION OF 442 DETRITAL-CLAY COATS

In this study, we have produced a high resolution, modern analogue data set and established
the distribution patterns of detrital-clay coats relative to surface sedimentary and biological
facies. Percentage clay fraction, grain size and bioturbation have all been advocated as
controls on the origin of clay coated grains in ancient, deeply buried sandstones.

447 Role of Grain Size

From this study, the observed inverse relationship of increasing detrital-clay coats coverage
with decreasing grain size (Fig. 10) is consistent with previous observations by Wilson
(1992), that clay coats are more extensively developed within finer grained sandstones in
Holocene eolian dune and marine-shelf settings. The Permian-Carboniferous Unayzah
sandstones, Saudi Arabia, also have a reported relationship between mean grain size and the

453 average percentage coverage of grains, with fine- to very fine-sandstone exhibiting the454 greatest degree of clay coat coverage (Shammari et al. 2010).

455 Role of Percentage Clay Fraction Control

456 The role that percentage clay fraction ( $< 2 \mu m$ ) plays in the formation and distribution of 457 detrital-clay coated grains is not well established within the literature. However, the Anllóns 458 Estuary, Spain, has a clay fraction percentage that increases in marginal areas towards the 459 upper tidal limit (Dowey 2013), consistent with the present study. The Anllóns example 460 identified a trend comparable with Ravenglass of increasing clay coats coverage with 461 increasing co-deposited clay fraction percentage (Dowey 2013). Furthermore, in the Texas 462 Gulf Coast at Galveston and within the Brazos River, virtually no clay-coated grains occur in 463 environments that are characterised by low suspended sediment concentrations (assumed here 464 to be proportional to the percentage clay fraction) (Matlack et al. 1989).

465

### Bioturbation Control

Sediment bioturbation (specifically ingestion and excretion) has been experimentally shown
to lead to the creation of clay coats on detrital sand grains (McIlroy et al. 2003; Needham et

al. 2006; Needham et al. 2004; Needham et al. 2005). This mechanism works through the

469 production of a mucus membrane on sand grains which then adheres finer clay-silt sized

470 sediment on to the sand grains.

471 In the present study, the distribution of clay-coated grains does not spatially correlate with the

degree of bioturbation observed in the estuary (compare Fig 3, 8 and see Fig. 10). It is also

area notable that a similar conclusion can be drawn from the Lower Cretaceous Missisauga

474 Formation, Scotian Basin, where the coverage of clay coated grains does not positively

- 475 correlate with the degree of bioturbation (Gould et al. 2012). The lack of correlation between
- 476 bioturbation and the degree of clay coated grains in this study may result from the limited

environmental grain size niche of the utilized lugworm biogenic proxy. To address this, a
focused study on the abundance distribution of estuarine macro- and microorganisms would
be required.

# 480 IMPLICATIONS FOR HYDROCARBON EXPLORATION

481

# Target Reservoir Quality Prospects

482 At depths > 3 km (temperatures > 90°C) pervasive authigenic quartz typically starts to

become a dominant cement in sandstones (Bloch et al. 2002). Such sandstones risk becoming

extensively quartz cemented if grain coats are absent, or poorly developed, upon grain

485 surfaces (Ajdukiewicz and Larese 2012).

486 Based upon the surface distribution patterns of detrital-clay coats presented here (Figs. 8-10), 487 the best prospects for anomalously high reservoir quality due to the presence of clay coated 488 grains in deeply buried sandstones (> 3km), should be sought within the fine sand sized 489 sediment that also contains approximately 5% clay fraction percentage. Specifically targeting 490 clay-bearing sandstones in the hunt for elevated porosity is against common convention, 491 which would typically target the cleanest, most clay-free sandstones. Our interpreted 492 optimum value of approximately 5 % clay fraction is based upon the likelihood of producing 493 extensive clay coats within sandstones. However we note that highly elevated clay content 494 would of course produce a detrimental effect on permeability and porosity (see next section). 495 Sites with fine sand-sized sediment that also contain approximately 5% clay fraction 496 correspond to inner estuary tidal bar, tidal flat and fluvial point bar facies in the Ravenglass 497 system. In contrast, coarse, clean sand from tidal channels, outer sand flat and foreshore 498 facies would, upon deep burial, potentially experience pervasive quartz cementation due to 499 the lack of inhibiting detrital-clay coated grains if the sediment reached temperatures 500 sufficient for quartz cementation.

# Goldilocks Zone of Optimum Detrital-Clay Coat Coverage

502	The high resolution, marginal-shallow marine model for the distribution of detrital clay-
503	coated grains presented in this study may be used, by analogy, to help in the prediction of
504	clay coated sandstones in the deep subsurface. Too much clay is highly detrimental to
505	sandstone reservoir quality (Armitage et al. 2016; Houseknecht and Pittman 1992; Worden
506	and Morad 2003) since abundant clay minerals fill pores and block pore throats between sand
507	grains. The quantity of clay in a sandstone that is sufficient to coat grains (and thus inhibit
508	quartz cement) but not enough to block pore throats, surprisingly, remains poorly resolved,
509	and is addressed below.
510	Bloch et al. (2002) noted that a minor amount of clay (as little as 1 to 2% of the rock volume)
511	can coat a relatively large surface area of sandstone grains, but the optimum amount for
512	specific clay minerals has not been precisely defined. Here examples from previous studies
513	were used to help constrain broad percentages of total clay quantities as clay coats that can
514	lead to the development of diagenetic coats which can successfully inhibit quartz cement.
515	Pittman et al. (1992) suggested an optimum range of 5 to 13 % sediment volume of clays
516	occurring as chlorite grain coats for the Tuscaloosa Formation and 4 to 7 % for the Berea
517	Sandstone. Heald and Baker (1977) reported an optimum range of 3.5 to 6.5 % volume of
518	illite clay coats for reservoir quality within the Rose Run sandstone.
519	Here, we tentatively propose (from the observed association of clay fraction occurring
520	predominantly as clay coatings) lower and upper threshold values of 3.5 and 13.0 % total

volume of clay minerals (chlorite, illite and mixed) as the optimum range for the eventual

beta development of clay coats that can form continuous barriers that prevent quartz cementation

and so preserve reservoir quality. Using the 3.5 to 13.0 % range of total volume of clays, we

524 have mapped out regions within the Ravenglass Estuary that would lead to the best reservoir

525	quality, were this sedimentary system to be deeply buried (Fig. 11). These optimum regions	s,
526	termed "Goldilocks zones", encompass the central tidal flat region, non-vegetated and upper	r
527	estuary tidal bar depositional environments.	
528	CONCLUSIONS	
529	1. The work presented here, from the Ravenglass Estuary, UK, represents the first high	l
530	resolution study of the distribution of detrital-clay coated grains within a modern	
531	marginal-shallow marine setting.	
532	2. Sedimentary environment is the main control on the absolute quantity of clay minera	als
533	and detrital-clay coat sand grain coverage in these sand-dominated sediments.	
534	3. Detrital-clay coats in recent sediments have discontinuous ridged, bridged and	
535	clumped textural morphologies. The coats on sand grains are formed of individual	
536	interlocking clay minerals with silt-sized lithic and bioclastic accessory components	
537	and were probably derived from a combination of infiltration (of clay-bearing water	
538	into sand-dominated sediment), flocculation and biogenic processes. Clay coats range	ge
539	from being absent to covering $> 30\%$ of sand grain surfaces in a given sample.	
540	4. The observation that the illite-chlorite-kaolinite clay coat mineralogy reflects the bul	lk
541	clay mineralogy of the estuary implies that the clay coats were formed in situ within	
542	the estuary rather than in the hinterland.	
543	5. The distribution of detrital-clay coated grains is primarily a function of sediment gra	in
544	size and clay fraction percentage. In the Ravenglass case study, a sediment	
545	assemblage composed of fine-grained sand containing $> 5$ % clay fraction percentage	e
546	is necessary for the development of uniform-well developed clay coats on detrital	
547	grains.	

- **6.** The best prospects for anomalously high reservoir quality in deeply buried marginal
- 549 marine sandstones (i.e. with inhibited growth of quartz cement) should most likely be
- 550 sought within clay-rich inner estuary tidal facies.

### 551 FIGURE CAPTIONS

552 Figure 1. Location maps. A) The Ravenglass Estuary, within the UK. B) Regional map

showing the study area and component depositional environments. Tidal flats have been

subdivided based upon their component clay fraction ( $< 2 \mu m$ ); 0-10 % sand flat, 10-30 %

555 muddy sand flat, 30-80 % sandy mud flat. Classification modified from the scheme initially

proposed by Dyer (1979). The black square indicates the sediment sample location from

557 which clay coat (SEM-EDS) and sediment clay fraction (XRD) mineralogical analyses (Fig.4

558 and Fig. 5) were undertaken.

559 Figure 2. SEM electron images showing the variable extent of attached clay coats observed

560 within surface sediment samples, which define the basis of the utilized classification scheme.

1) Complete absence of clay coats. 2) ~1 to 5 % attached clays on less than half of the grains.

562 3) Every grain exhibits ~5 to 15 % clay coats coverage. 4) Clay coats observed on every grain

with the majority exhibiting extensive ~15 to 30 % coverage. 5) Extensive, > 30 % clay

564 coats coverage observed upon every grain.

565 Figure 3. Distribution maps of surface sedimentary features. A) High resolution map of

surface sediment grain size (n = 3150). B) Surface distribution of clay fraction percentage (n

567 = 2000) C) High resolution map of lugworm population in surface sediment (n = 3182).

Figure 4. X-ray diffractogram used to quantify the bulk sediment clay fraction mineralogy of
surface sediment within the Ravenglass Estuary (for location, see Fig. 1).

570 Figure 5. Representative SEM electron images of the textural characteristics of surface clay

571 coated sand grains. Arrows indicate regions of clay coat coverage. Note the extent of the

ridged clay coat morphologies composed of interlocking and aligned clay particles (A, B, C,

and E). The clumped clay coat aggregates composed of clay minerals, lithics and organics

are illustrated within (A, D, G, and F). The textural clay coat characteristic of extending pore

ward are observed within (A, C and F) and with greatest accumulation (thickness) observed
within grain indentations (E and G).

577 Figure 6. Clay coat textures showing the main morphological feature classification observed 578 within surface sediment samples. A) Ridged clay coat. B) Bridged clay coat structure. C) 579 Clumped clay coat. Note greatest thickness of attached coating within the grain indentation 580 (enlarged in F). Arrows indicate regions of clay coat coverage. 581 Figure 7. Scanning electron microscope-energy dispersive spectrometry (SEM-EDS) image, 582 showing clay coat and bulk sediment mineralogy for within muddy sand flat sediment (for 583 location, see Fig. 1). A) Backscattered electron image. B) SEM-EDS image of framework 584 grain mineralogy. C) SEM-EDS image of the component clay fraction mineralogy. D to F) 585 SEM-EDS images of the distribution of illite, chlorite, and kaolinite. Arrows indicate regions 586 of attached clay coating. 587 Figure 8. Distribution map of surface clay coated sand grains within the Ravenglass Estuary 588 (n = 195). Plotted are the surface distribution of classified areas in light grey signify at least

partial clay coat coverage, with dark grey-black regions indicating extensive surface claycoated sand grains.

591 Figure 9. Frequency histograms for all sediment samples, divided by depositional

environment and clay coat bin class: (A) Total number of samples in each clay coat class. (B)

593 Normalised data to reveal relative importance of different environments for optimum clay

coat coverage. Clay coat class 1 and 2 have minimal to compete absence of clay coats.

595 Figure 10. Average grain size, lugworm population and clay fraction percentage plots for

596 each representative clay coat bin class.

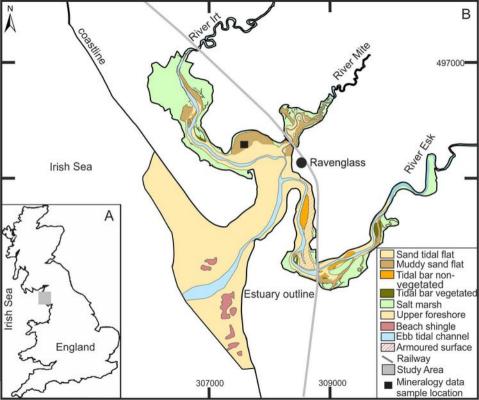
- 597 Figure 11. Distribution map indicating the literature-constrained Goldilocks zone of the
- 598 optimum quantity of total clay (i.e. detrital-clay coated sand grains inhibiting quartz cement
- 599 but not blocking pore throats).

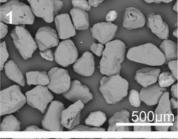
### 600 **REFERENCES**

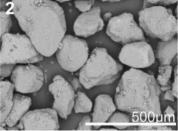
601 AAGAARD, P., JAHREN, J.S., HARSTAD, A.O., NILSEN, O., AND RAMM, M., 2000, Formation of grain-coating 602 chlorite in sandstones. Laboratory synthesized vs. natural occurrences: Clay Minerals, v. 35, 603 p. 261-269. 604 AINSWORTH, R.B., VAKARELOV, B.K., AND NANSON, R.A., 2011, Dynamic spatial and temporal prediction of 605 changes in depositional processes on clastic shorelines: toward improved subsurface 606 uncertainty reduction and management: AAPG bulletin, v. 95, p. 267-297. 607 AJDUKIEWICZ, J.M., AND LARESE, R.E., 2012, How clay grain coats inhibit quartz cement and preserve 608 porosity in deeply buried sandstones: Observations and experiments: American Association 609 of Petroleum Geologists Bulletin, v. 96, p. 2091-2119. 610 AJDUKIEWICZ, J.M., NICHOLSON, P.H., AND ESCH, W.L., 2010, Prediction of deep reservoir quality using 611 early diagenetic process models in the Jurassic Norphlet Formation, Gulf of Mexico: 612 American Association of Petroleum Geologists Bulletin, v. 94, p. 1189-1227. 613 AL-RAMADAN, K.A., HUSSAIN, M., IMAM, B., AND SANER, S., 2004, Lithologic characteristics and diagenesis 614 of the Devonian Jauf sandstone at Ghawar Field, eastern Saudi Arabia: Marine and 615 Petroleum Geology, v. 21, p. 1221-1234. 616 ARMITAGE, P.J., WORDEN, R.H., FAULKNER, D.R., BUTCHER, A.R., AND ESPIE, A.A., 2016, Permeability of the 617 Mercia Mudstone: suitability as caprock to carbon capture and storage sites: Geofluids, v. 618 16, p. 26-42. 619 BILLAULT, V., BEAUFORT, D., BARONNET, A., AND LACHARPAGNE, J.C., 2003, A nanopetrographic and textural 620 study of grain-coating chlorites in sandstone reservoirs: Clay Minerals, v. 38, p. 315-328. 621 BLOCH, S., LANDER, R.H., AND BONNELL, L., 2002, Anomalously high porosity and permeability in deeply 622 buried sandstone reservoirs: Origin and predictability: American Association of Petroleum 623 Geologists Bulletin, v. 86, p. 301-328. 624 BOUSHER, A., 1999, Ravenglass Estuary: Basic characteristics and evaluation of restoration options, 625 Restrad-Td. 626 COCKER, J., KNOX, W., LOTT, G., AND MILODOWSKI, A., 2003, Petrologic controls on reservoir quality in the 627 Devonian Jauf Formation sandstones of Saudi Arabia: Geofrontier, v. 1, p. 6-11. 628 CRONE, A.J., 1975, Laboratory and field studies of mechanically infiltrated matrix clay in arid fluvial 629 sediments, University of Colorado. 630 DANESHVAR, E., 2011, Role of provenance on clay minerals and their distribution in modern estuaries: 631 University of Liverpool, 236 p. 632 DANESHVAR, E., AND WORDEN, R.H., 2016, Feldspar alteration and Fe minerals: origin, distribution and 633 implications for sandstone reservoir quality in estuarine sediments. In: Armitage, P. J., 634 Butcher, A. R., Churchill, J. M., Csoma, A. E., Hollis, C., Lander, R. H., Omma, J. E. & Worden, 635 R. H. (eds) 2016. Reservoir Quality of Clastic and Carbonate Rocks: Analysis, Modelling and 636 Prediction. : Geological Society, London, Special Publications, v. 435. 637 DOWEY, P.J., 2013, Prediction of clay minerals and grain coatings in sandstone reservoirs utilising 638 ancient examples and modern analogue studies: University of Liverpool. 639 DOWEY, P.J., HODGSON, D.M., AND WORDEN, R.H., 2012, Pre-requisites, processes, and prediction of 640 chlorite grain coatings in petroleum reservoirs: A review of subsurface examples: Marine and 641 Petroleum Geology, v. 32, p. 63-75.

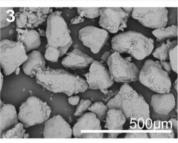
642 643	DYER, K.R., 1979, Estuarine hydrography and sedimentation: a handbook, Cambridge University Press Cambridge.
644	EHRENBERG, S.N., 1993, Preservation of anomalously high-porosity in deeply buried sandstones by
645	grain coating chlorite - examples from the Norwegian continental shelf: American
646	Association of Petroleum Geologists Bulletin, v. 77, p. 1260-1286.
647	EHRENBERG, S.N., 1997, Influence of depositional sand quality and diagenesis on porosity and
648	permeability: Examples from Brent Group Reservoirs, northern North Sea (vol 67, pg 202,
649	1997): Journal of Sedimentary Research, v. 67, p. 618-618.
650	FRANKS, S.G., AND ZWINGMANN, H., 2010, Origin and timing of late diagenetic illite in the Permian-
651	Carboniferous Unayzah sandstone reservoirs of Saudi Arabia: American Association of
652	Petroleum Geologists Bulletin, v. 94, p. 1133-1159.
653	GAUPP, R., AND OKKERMAN, J.A., 2011, Diagenesis and reservoir quality of Rotliegend Sandstones in the
654	Northern Netherlands - A review, <i>in</i> Grotsch, J., and Gaupp, R., eds., Permian Rotliegend of
655	the Netherlands: Society for Sedimentary Geology Special Publication, p. 193-226.
656	GOULD, K., PE-PIPER, G., AND PIPER, D.J.W., 2010, Relationship of diagenetic chlorite rims to
657	depositional facies in Lower Cretaceous reservoir sandstones of the Scotian Basin:
658	Sedimentology, v. 57, p. 587-610.
659	GOULD, K.M., PIPER, D.J.W., AND PE-PIPER, G., 2012, Lateral variation in sandstone lithofacies from
660	conventional core, Scotian Basin: implications for reservoir quality and connectivity:
661	Canadian Journal of Earth Sciences, v. 49, p. 1478-1503.
662	GRIGSBY, J.D., 2001, Origin and growth mechanism of authigenic chlorite in sandstones of the lower
663	Vicksburg Formation, south Texas: Journal of Sedimentary Research, v. 71, p. 27-36.
664	HEALD, M.T., AND BAKER, G.F., 1977, Diagenesis of Mt Simon and Rose Run Sandstones in western
665	West Virginia and southern Ohio: Journal of Sedimentary Petrology, v. 47, p. 66-77.
666	HOUSEKNECHT, D.W., 1992, Clay minerals in Atokan deep-water sandstone facies, Arkoma basin:
667	origins and influence on diagenesis and reservoir quality.
668	HOUSEKNECHT, D.W., AND PITTMAN, E.D., 1992, Origin, diagenesis and petrophysics of clay minerals in
669	sandstones SEPM Special Publication: Tulsa Oklahoma, Society of Economic Paleontologists
670	and Mineralogists.
671	JERNIGAN, D.L., AND MCATEE, J.L., 1975, Critical point drying of electron microscope samples of clay
672	minerals: Clays and Clay Minerals, v. 23, p. 161-162.
673	LANDER, R.H., LARESE, R.E., AND BONNELL, L.M., 2008, Toward more accurate quartz cement models: The
674	importance of euhedral versus noneuhedral growth rates: American Association of
675	Petroleum Geologists Bulletin, v. 92, p. 1537-1563.
676	LLOYD, J.M., ZONG, Y., FISH, P., AND INNES, J.B., 2013, Holocene and Lateglacial relative sea-level change
677	in north-west England: implications for glacial isostatic adjustment models: Journal of
678	Quaternary Science, v. 28, p. 59-70.
679	LUO, J.L., MORAD, S., SALEM, A., KETZER, J.M., LEI, X.L., GUO, D.Y., AND HLAL, O., 2009, Impact of diagenesis
680	on reservoir quality evolution in fluvial and lacustrine-deltaic sandstones: evidence from
681	Jurassic and Triassic sandstones from the Ordos Basin, China: Journal of Petroleum Geology,
682	v. 32, p. 79-102.
683	MATLACK, K.S., HOUSEKNECHT, D.W., AND APPLIN, K.R., 1989, Emplacement of clay into sand by
684	infiltration: Journal of Sedimentary Petrology, v. 59, p. 77-87.
685	MCILROY, D., WORDEN, R.H., AND NEEDHAM, S.J., 2003, Faeces, clay minerals and reservoir potential:
686	Journal of the Geological Society, v. 160, p. 489-493.
687	MOHAN KESSARKAR, P., PURNACHANDRA RAO, V., SHYNU, R., MEHRA, P., AND VIEGAS, B.E., 2010, The nature
688	and distribution of particulate matter in the Mandovi estuary, central west coast of India:
689	Estuaries and coasts, v. 33, p. 30-44.
690	MORAD, S., AL-RAMADAN, K., KETZER, J.M., AND DE ROS, L.F., 2010, The impact of diagenesis on the
691	heterogeneity of sandstone reservoirs: A review of the role of depositional facies and

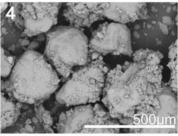
692	sequence stratigraphy: American Association of Petroleum Geologists Bulletin, v. 94, p.
693	1267-1309.
694	MORAES, M.A.S., AND DE ROS, L.F., 1992, Depositional, infiltrated and authigenic clays in fluvial
695	sandstones of the Jurassic Sergie Formation, Reconcavo Basin, northeastrn Brazil: In: Origin,
696	diagenesis and petrophysics of clay minerals in sandstones (eds. Houseknecht, D.W. and
697	Pittman, E.D.) SEPM Special Publication, v. 47, p. 197-208.
698	MOSELEY, F., 1978, The Geology of the Lake District, Occoasional Publication: Leeds, Yorkshire
699	Geological Society, p. 284.
700	NEEDHAM, S.J., WORDEN, R.H., AND CUADROS, J., 2006, Sediment ingestion by worms and the production
701	of bio-clays: a study of macrobiologically enhanced weathering and early diagenetic
702	processes: Sedimentology, v. 53, p. 567-579.
703	NEEDHAM, S.J., WORDEN, R.H., AND MCILROY, D., 2004, Animal-sediment interactions: the effect of
704	ingestion and excretion by worms on mineralogy: Biogeosciences, v. 1, p. 113-121.
705	NEEDHAM, S.J., WORDEN, R.H., AND MCILROY, D., 2005, Experimental production of clay rims by
706	macrobiotic sediment ingestion and excretion processes: Journal of Sedimentary Research,
707	v. 75, p. 1028-1037.
708	OZKAN, A., CUMELLA, S.P., MILLIKEN, K.L., AND LAUBACH, S.E., 2011, Prediction of lithofacies and reservoir
709	quality using well logs, Late Cretaceous Williams Fork Formation, Mamm Creek field,
710	Piceance Basin, Colorado: American Association of Petroleum Geologists Bulletin, v. 95, p.
711	1699-1723.
712	PIERCE, J., AND NICHOLS, M.M., 1986, Change of particle composition from fluvial into an estuarine
713	environment: Rappahannock River, Virginia: Journal of coastal research, p. 419-425.
714	PITTMAN, E.D., LARESE, R.E., AND HEALD, M.T., 1992, Clay coats: occurrence and relevance to
715	preservation of porosity in sandstones: In: Origin, diagenesis and petrophysics of clay
716	minerals in sandstones (eds. Houseknecht, D.W. and Pittman, E.D.) SEPM Special Publication,
717	v. 47, p. 241-255.
718	SANTOS, I.R., EYRE, B.D., AND HUETTEL, M., 2012, The driving forces of porewater and groundwater flow
719	in permeable coastal sediments: A review: Estuarine, Coastal and Shelf Science, v. 98, p. 1-
720	15.
721	SHAMMARI, S., FRANKS, S., AND SOLIMAN, O., 2010, Depositional and Facies Controls on
722	Infiltrated/Inherited Clay Coatings: Unayzah Sandstones, Saudi Arabia: GEO 2010.
723	STORVOLL, V., BJORLYKKE, K., KARLSEN, D., AND SAIGAL, G., 2002, Porosity preservation in reservoir
724	sandstones due to grain-coating illite: a study of the Jurassic Garn Formation from the Kristin
725	and Lavrans fields, offshore Mid-Norway: Marine and Petroleum Geology, v. 19, p. 767-781.
726	WILSON, M.D., 1992, Inherited grain-rimming clays in sandstones from eolian and shelf environments:
727	their origin and control on reservoir properties: In: Origin, diagenesis and petrophysics of
728	clay minerals in sandstones (eds. Houseknecht, D.W. and Pittman, E.D.) SEPM Special
729	Publication, v. 47, p. 209-225.
730	WISE, S., SMELLIE, J., AGHIB, F., JARRARD, R., AND KRISSEK, L., 2001, Authigenic smectite clay coats in CRP-3
731	drillcore, Victoria Land Basin, Antarctica, as a possible indicator of fluid flow: a progress
732	report: Terra Antartica, v. 8, p. 281-298.
733	WORDEN, R.H., AND MORAD, S., 2000, Quartz cementation in sandstones: a review of the key
734	controversies In: Quartz cementation in sandstones (eds. Worden, R.H. and Morad, S.)
735	International Association of Sedimentologists Special Publications, p. 1-20.
736	WORDEN, R.H., AND MORAD, S., 2003, Clay minerals in sandstones: Controls on formation, distribution
737	and evolution: In: Clay mineral cements in sandstones (eds. Worden, R.H. and Morad, S.)
738	International Association of Sedimentologists Special Publications, v. 34, p. 3-41.

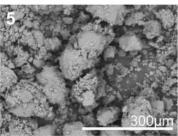


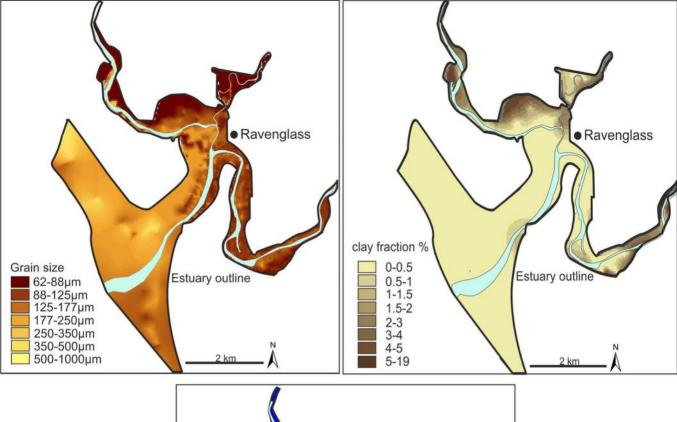


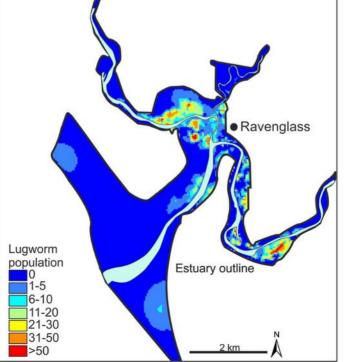


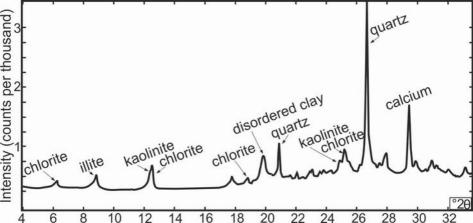


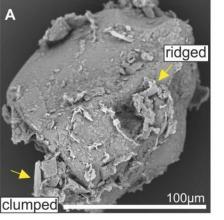


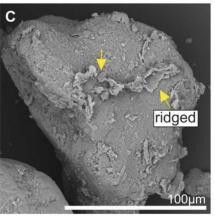


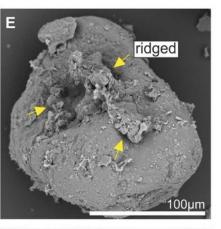


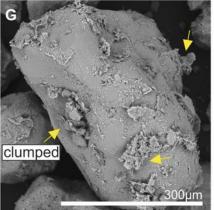


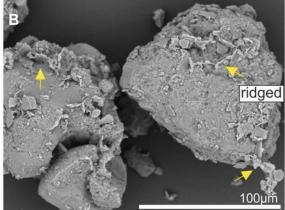


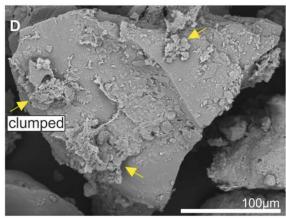


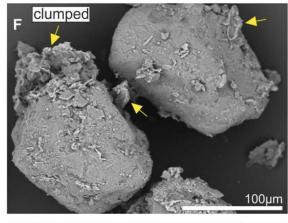


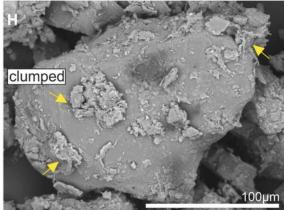


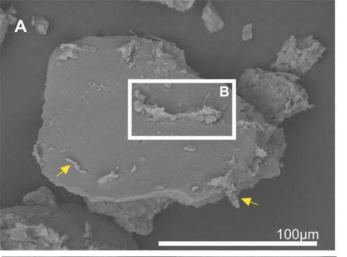


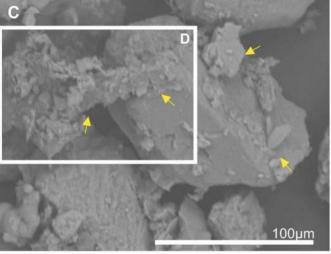


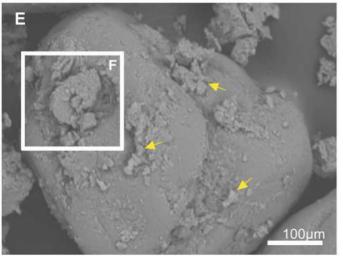


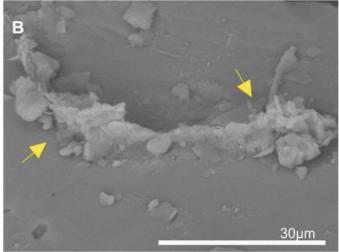


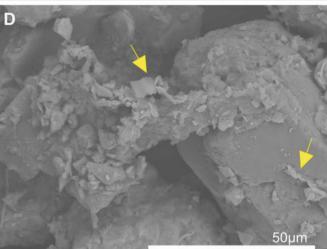


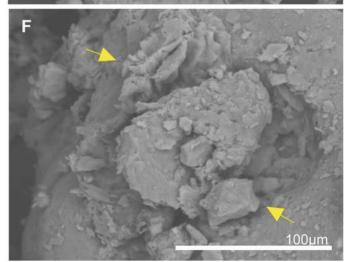


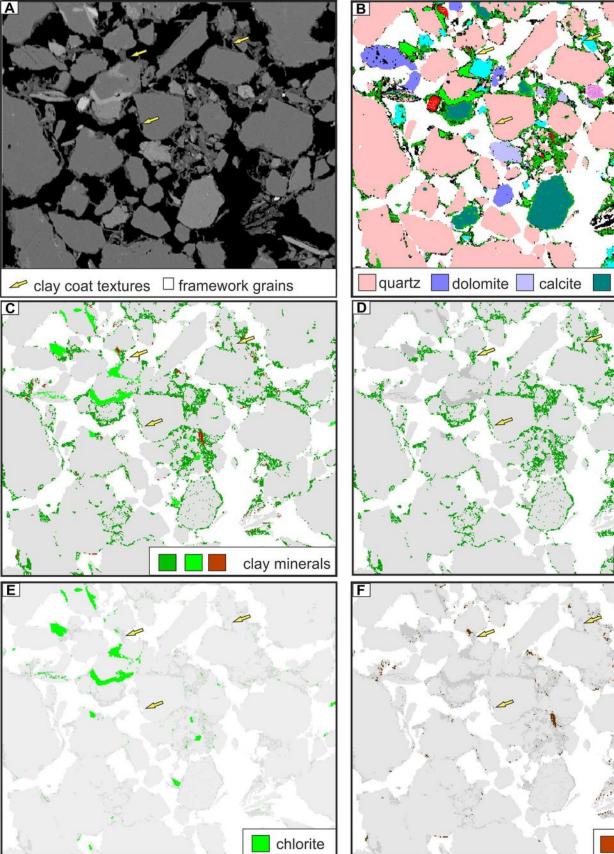












kaolinite

illite

feldspar

